A Low-Cost Differentially Driven Dual-Polarized Patch Antenna by Using Open Loop Resonators

Le-Hu Wen, Steven Gao, Qi Luo, Qingling Yang, Wei Hu, and Yingzeng Yin

***Abstract*—A novel differentially driven dual-polarized patch antenna is presented in this communication. The proposed antenna is a low-cost design with a simple configuration, which avoids using the conventional high cost multi-layer PCB technology. The antenna is composed of two intersected open loop resonators, which are connected to each other at the center. By using the electric coupling from the intersected resonators, two orthogonal radiating modes are excited from the top radiating patch. With the even and odd mode current distributions on the intersected resonators, high port isolation and low cross-polarization level are obtained. The external quality factor of the resonator is illustrated by using the analytical model of a double loaded resonator. To demonstrate the design method, the proposed antenna and array are designed, fabricated, and measured. Compared to the traditionally designed capacitively coupled antenna, two times wider impedance bandwidth is obtained for the proposed antenna with high isolation (>38.5 dB) and low cross-polarization level (<-33 dB). The antenna array is designed for 5G base stations, which features the compact size and low reflection coefficient (<-15 dB). In addition, beam scanning performance of the antenna array is also investigated for base station applications.**

***Index Terms*—Differentially driven antenna, dual-polarized antenna, open loop resonators.**

I. Introduction

As the development of wireless communication systems, dual-polarized antennas have gained widely applications because of the advantages of increased communication channel capacity and reduced multipath fading effect. In addition, dual-polarized antennas, with low profile and wideband characteristics, are highly desirable in the increasingly spaced-limited application scenarios, such as base stations, radars, satellites, etc. Owing to these advantages and different requirements, dual-polarized antennas are intensively researched and continuously developed in recent years [1]. To realize dual-polarization, patch antennas [2]-[8] and crossed dipole antennas [9]-[15] are the commonly used antenna types. However, antennas in the designs [2]-[8] use multi-layer PCB technology, which leads to the complicated manufacture process and increased fabrication cost. With wide impedance bandwidth and simple configuration, dual-polarized crossed dipole antennas [9]-[15] are presented for base station applications. However, these antennas normally have high profiles, and they are not easy to be integrated with the other passive and active microwave devices.

Recently, differential microwave circuits are widely applied in wireless communication systems because of the advantages of reduced noise level, increased harmonic suppression, and enhanced common-mode rejection [16]. In the differential circuit systems, differentially driven antennas are much preferable compared to the conventional single-ended antennas. If the differentially driven antenna is replaced by the traditional single-ended antenna, an additional balun or an out-of-phase power divider will be placed between the two different interfaces. Undesired insertion loss and impedance mismatching will be introduced. Accordingly, differentially driven antennas [17]-[23] are developed to meet these requirements. In [21], a wideband differentially driven dual-polarized antenna is proposed with the impedance bandwidth of 19%. However, due to the complicated three layers structure and different via holes configuration, the antenna is of high cost. In addition, the measured cross-polarization level is only -16 dB in the broadside direction. By using 180º ring hybrid coupler, the differentially driven antenna in [23] achieves high isolation (higher than 62 dB) and low cross-polarization (lower than -50 dB), but its impedance bandwidth is quite narrow.

In this communication, a novel low-cost differentially driven dual-polarized patch antenna by using the intersected open loop resonators is proposed. By using the electric coupling from the intersected resonators to the top radiating patch, two orthogonal polarizations are realized. With the even and odd mode current distributions on the intersected resonators, high port isolation and low cross-polarization level are achieved. The proposed dual-polarized antenna is further illustrated by the resonator-based filtering antenna design method. The differentially driven resonator can be equivalent as a double loaded resonator, and the external quality factor is extracted based on the double loaded resonator. Compared to the traditional multi-layer patch antennas, the proposed antenna has the advantages of simple configuration with low fabrication cost.

To validate the design method, the proposed antenna and array are designed, fabricated, and measured. For the antenna element, wide impedance bandwidth of 17.2% is measured with the overall thickness of $0.067\lambda_0$ (where λ_0 is the free space wavelength at 3.5 GHz). Furthermore, high isolation (>38.5 dB) and low cross-polarization level (< -33 dB) are achieved. For the dual-polarized 1×4 antenna array, which is designed for 5G base station applications with very low reflection coefficient (<-15 dB). The measured half-power beamwidth within the bandwidth is 66-70º and 20-22º in H-plane and V-plane, respectively. In addition, beam scanning performance is also investigated for base station coverage.

II. Antenna Element

A. Configuration

The configuration of the proposed differentially driven dual-polarized antenna is shown in Fig. 1. The antenna is composed of three parts, a top square radiating patch, two intersected open loop resonators, and a square ground plane. The top radiating patch operates at the dominant mode (TM_{10} mode) for each polarization. Hence, the length of the square patch is about half guided wavelength at the center frequency. For the open loop resonators, the total length ((L1+L2+L3)×2) is about half free-space wavelength at the center frequency.

The radiating patch is printed on a substrate of Rogers 4003C, with the relative dielectric permittivity of 3.55 and the thickness of 0.813 mm. The intersected open loop resonators are etched from a copper sheet with the thickness of 0.1 mm. These two open loop resonators are connected to each other at the center of each resonator, and four feed ports are connected to the intersected resonators with the distance of L4×2. The height from the top substrate to the ground

This work was in part supported by EPSRC grants EP/N032497/1 and EP/P015840/1, and in part by scholarship from the China Scholarship Council (No. 201706960013).

Lehu Wen is with the School of Engineering and Digital Arts, University of Kent, Canterbury, CT2 7NT, U.K. (e-mail: lw347@kent.ac.uk)

S. Gao, Q. Luo, and Q. Yang are with the University of Kent, Canterbury, CT2 7NT, U.K. (e-mail: s.gao@kent.ac.uk).

W. Hu and Y. Yin are with the National Key Laboratory of Antennas and Microwave Technology, Xidian University, Xian, 710071, China.

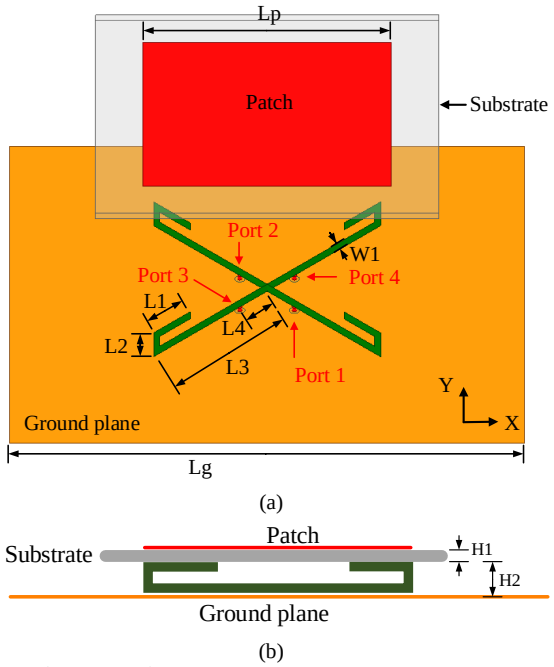

Fig. 1. Configuration of the proposed dual-polarized antenna. (a) Exploded view. (b) Side view. (Detailed antenna design parameters: L1 = 6 mm, L2 = 3.4 mm, L3 = 18.7 mm, L4 = 4.5 mm, W1= 1 mm, Lp = 29 mm, Lg= 80 mm, H1 = 0.813 mm, H2 = 5 mm.)

plane is 5 mm. It should be noted that the antenna is designed for ±45º polarizations. Therefore, as a general definition for radiation patterns, the xz-plane in Fig. 1 is defined as H-plane (horizontal plane), and the yz plane is defined as V-plane (vertical plane).

The pair of port 1 and port 2 in the figure is designated as the differential port d1, while the pair of port 3 and port 4 is designated as the differential port d2. According to the mixed-mode scattering parameters analysis and calculation method in [24], the S-parameters of the differentially driven antenna are expressed as

$$S_{dd11} = (S_{11} + S_{22} - S_{12} - S_{21})/2 \quad (1)$$

$$S_{dd21} = (S_{31} + S_{42} - S_{32} - S_{41})/2 \quad (2)$$

where S_{ij} $(i = 1,2,3,4;\ j = 1,2,3,4)$ are the single-ended S-parameters, which can be obtained from the simulated or the measured results. By using the equations (1)-(2), one can get the differential S-parameters to illustrate the input impedance characteristic of the differentially driven antenna. All the simulation results are obtained by using the 3D electromagnetic simulation software ANSYS HFSS. The design parameters of the dual-polarized antenna are given in the caption of Fig. 1.

B. Working Principle

To illustrate the working principle of the proposed antenna, the resonator-based coupling structure for the differentially driven antenna is shown in Fig. 2. Owing to the symmetry of the antenna, only one polarization is illustrated. In the figure, resonator 1 represents the open loop resonator, resonator 2 denotes the top radiating patch. Note that the resonator 1 is driven by the differential pair of port 1 and port 2. The coupling coefficient (M_{12}) and the external quality factor (Q_e) can be synthesized by using the filter and filtering antenna design methods presented in [25]-[26]. A filtering response with FBW=15% and S_{11}<-15 dB is used for the initial antenna design, and the synthesized M_{12} and Q_e are 0.215 and 5.565, respectively.

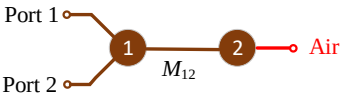

Fig. 2. Coupling structure of the proposed antenna for one polarization.

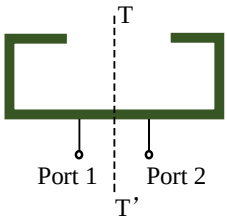

Fig. 3. Double loaded open loop resonator for one polarization.

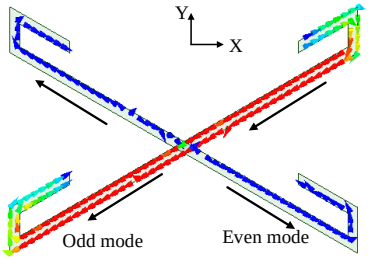

Fig. 4. Surface current distribution on the open loop resonators.

The external quality factor for the differentially driven resonator is different from the traditionally designed singly driven resonator. Because of the loading of the two differential ports, one can get the following relation

$$S_{21} = \frac{1}{1 + jQ_e\Delta\omega/\omega_0} \quad (3)$$

then, the external quality factor for the differentially driven antenna can be derived as

$$Q_e = \frac{\omega_0}{\Delta\omega_{3dB}} \quad (4)$$

where ω_0 is the resonant frequency, $\Delta\omega_{3dB}$ is the bandwidth at which the attenuation for S_{21} is 3 dB lower than the resonant frequency. Therefore, the relation between the distance of the two differential feed ports (2 × L4) and the external quality factor (Q_e) can be obtained by using (3)-(4). With the relation of L4 and Q_e, and referring to the initial value of Q_e=5.565, an initial feed position of L4 can be determined for the antenna design.

The symmetrical plane of the excited resonator can be equivalent to a virtual ground plane. As shown in Fig. 3, TT' plane is a symmetrical plane of the resonator. Because of the differentially driven method, odd mode current is distributed on the φ =45º arranged resonator, and the symmetrical plane (TT') represents the short circuit plane. This will be further demonstrated by the simulated current distribution on the resonators. Fig. 4 shows the current distribution on the surface of the open loop resonators at 3.5 GHz. Strong current distribution can be observed on the φ=45º excited resonator with the same current direction, and it is an odd mode current distribution. The strongest magnitude is located at the center of the resonator, and the weakest current magnitude is distributed on the both ends of the resonator. Therefore, the top radiating patch is excited by the open loop resonator with electric coupling. Whereas the φ=-45º unexcited resonator, reverse current direction (which is the even mode current distribution) is observed with very weak current distribution. The symmetrical TT' plane for this resonator is equivalent to an open circuit plane. By virtue of the short circuit plane and the open circuit plane, there will be no

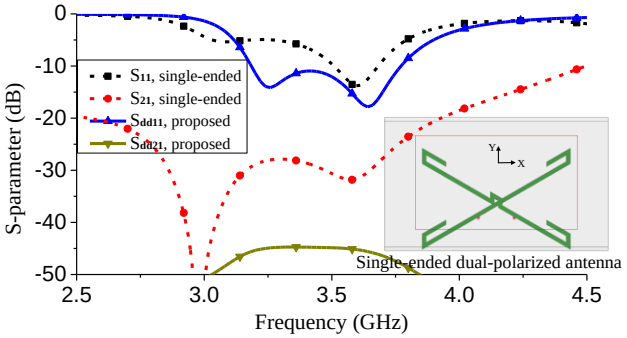

Fig. 5. Simulated S-parameters between the single-ended and differentially driven dual-polarized antenna.

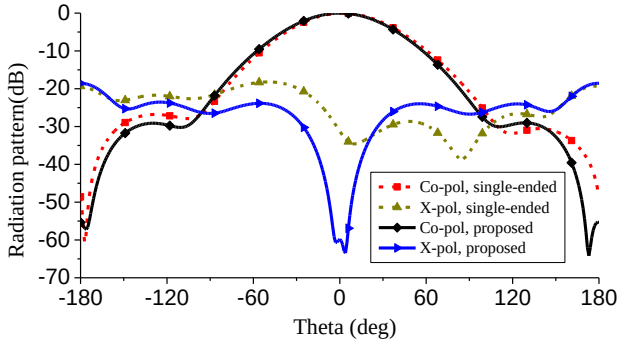

Fig. 6. Simulated normalized H-plane radiation patterns for the single-ended and differentially driven dual-polarized antenna.

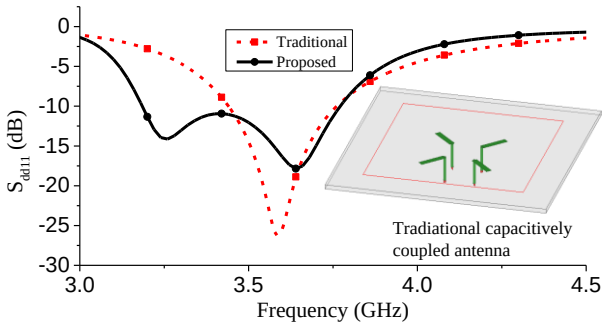

Fig. 7. Comparison between the traditional capacitively coupled antenna and the proposed antenna.

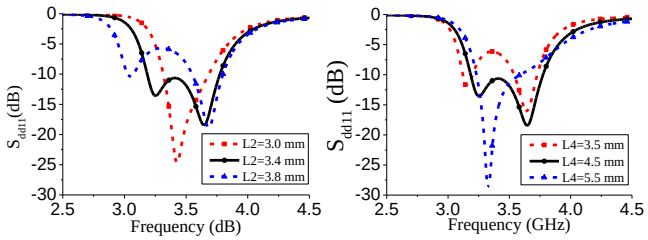

Fig. 8. Parametric studies of the proposed dual-polarized antenna by changing the values of (a) L2. (b) L4.

influence on each other's resonance, even though the resonators are connected to each other at the center. The current distribution on the intersected resonators also reveals that high port isolation and low cross-polarization level can be obtained for the two orthogonal polarizations.

A single-ended antenna is compared with the proposed differentially driven antenna to illustrate the high isolation and low cross-polarization of the proposed antenna. Both of them are excited by the open loop resonators. The simulation model of the single-ended dual-polarized antenna is inset into the bottom right corner of Fig. 5. Different from the proposed antenna, the two resonators are crossed but not connected to each other to avoid the mutual influence of the dominant resonant modes on the two open loop resonators. Therefore, there is a crossover bridge at the center of the φ=-45° arranged resonator. Two feed ports are connected to the two crossed open loop resonators with the same feed position as the differentially driven antenna in Fig. 1.

As shown in Fig. 5, two obvious differences can be observed. First, the reflection coefficient for the single-ended dual-polarized antenna is deteriorated, which results from different loading effects of external quality factors, as illustrated by (4). The single-ended reference antenna becomes a single loaded dual-polarized antenna. The simulated isolations for two antennas are also different. The simulated isolation for the single-ended dual-polarized antenna is 31 dB within the bandwidth due to the loss of the symmetrical driven ports, while the isolation of the differential driven dual-polarized antenna is higher than 45 dB owing to the symmetrical differentially driven ports.

The simulated normalized H-plane radiation patterns for the single-ended and differentially driven dual-polarized antennas are shown in Fig. 6. The co-polarized radiation patterns are almost the same. However, the simulated cross-polarization of the single-ended reference antenna is unsymmetrical. Whereas the cross-polarization of the differentially driven antenna is symmetrical, and it is much lower in the broadside direction owing to the symmetrical differential excitation.

C. Bandwidth Enhancement

Owing to the introduction of the intersected open loop resonators, the proposed differentially driven dual-polarized antenna has a wider impedance bandwidth compared to the traditionally designed capacitively coupled antenna. The configuration of the traditionally designed capacitively coupled antenna is inset into the bottom right corner of Fig. 7. The capacitive coupling is introduced by using the copper strips (in green colour) on the bottom layer of the substrate. The copper strips on the bottom layer can also be regarded as the coupling probes to feed the top radiating patch. It is also designed as a differentially driven antenna for good comparison. Both the capacitively coupled antenna and the proposed antenna have the same height and patch size.

As shown in Fig. 7, the simulated impedance bandwidth for $S_{11} < -10$ of the capacitively coupled antenna is 3.45-3.76 GHz (FBW= 8.3%) with a deep reflection zero at 3.6 GHz. One resonance is observed, which is from the top radiating patch. The proposed antenna has an impedance bandwidth of 3.16-3.74 GHz (FBW= 16.8%). Two times wider bandwidth is obtained for the proposed dual-polarized antenna with two reflection zeroes at 3.26 GHz and 3.64 GHz. Two resonances are observed, and they are generated from the top radiating patch and the open loop resonator. Because the simulated isolations of these two antennas are higher than 45 dB, they are not included in the figure for comparison.

D. Parametric Study

To investigate the effect of the antenna parameters on the antenna input impedance, parametric studies are performed. The antenna bandwidth is sensitive to the intersected resonators, including the length of resonators, the coupling strength, and the feed position. In Fig. 1, it can be seen that the length of the resonator and the coupling strength can be controlled by L2, and the feed position is controlled

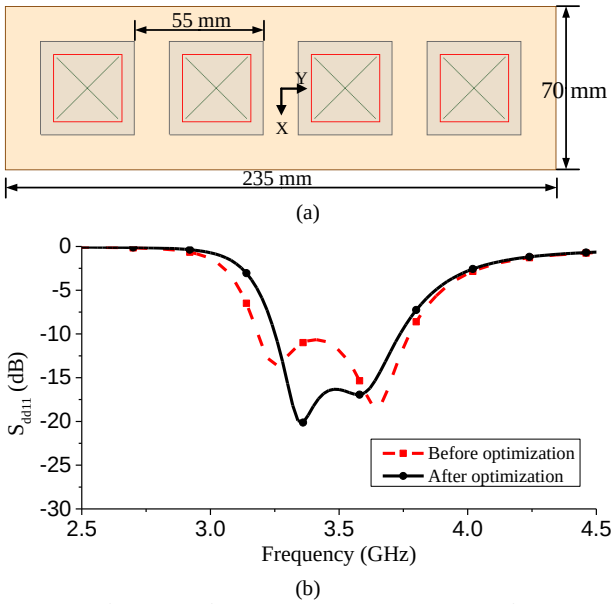

Fig. 9. (a) Configuration of the dual-polarized antenna array for base station $\pm 45^{\circ}$ polarizations. (b) The simulated reflection coefficients before and after optimization. (Optimized antenna element parameters: L1=5.8 mm, L2= 3.2 mm, others are unchanged.)

by L4. Hence, these two parameters are studied to investigate the effects of the open loop resonators on the antenna performance. Note that when one parameter is studied, the other parameters keep unchanged.

Fig. 8 (a) shows the simulated reflection coefficient with different L2. The length of L2 has two effects on the antenna performance. The first is the length of the resonator. Then, more importantly, is the coupling strength between the top radiating patch and the open loop resonator. Therefore, when increasing L2, two resonances are departed and the reflection coefficient is deteriorated. In Fig. 8 (b), the variance of the reflection coefficient is more complicated. As illustrated by (4), the feed position affects the external quality factor of the resonator. Hence, the variance of L4 will change the impedance bandwidth of the antenna and shift the resonances of the antenna. From the studies of these antenna parameters, optimization can be performed to obtain the best impedance bandwidth for the proposed dual-polarized antenna.

III. Antenna Array

In this section, a 1×4 linear array is designed for base station applications. To meet the requirements for base stations [9], such as the very low reflection coefficient (<-15 dB) and specific half-power beamwidth (within 60º-70º), the antenna element needs to be further optimized. As shown in Fig. 9 (a), the optimized total size of the 1×4 antenna array is 235 mm×70 mm, with the element distance of 55 mm. The distance between the elements is $0.64\lambda_0$ (λ_0 is the wavelength in the free space at 3.5 GHz), which is designed to eliminate the possible grating lobes and ensure the beam scanning performance of base stations [27].

The parameters for the array element are shown in the caption of Fig. 9, while other parameters are the same as the ones presented in the last section. Fig. 9 (b) compares the antenna reflection coefficients before and after optimization. After optimization, the simulated bandwidth for $S_{dd11} < -15$ dB is 3.28-3.64 GHz. Because the simulated isolations of both two antennas are higher than 45 dB, they are not included in the figure for comparison.

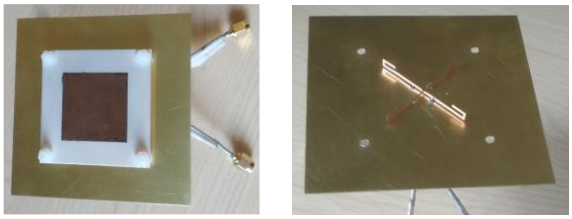

Fig. 10. Photographs of the fabricated dual-polarized antenna prototype. (a) Top view. (b) Inside view of the intersected open loop resonators.

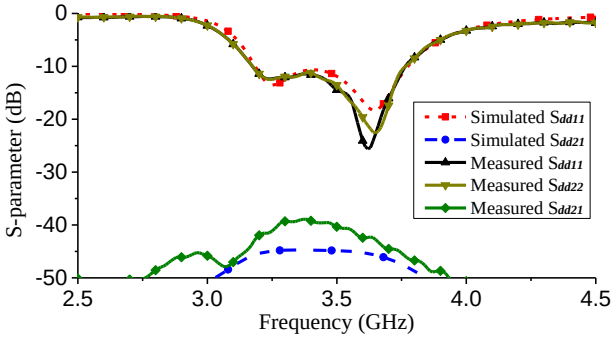

Fig. 11. Measured and simulated S-parameters of the fabricated antenna element.

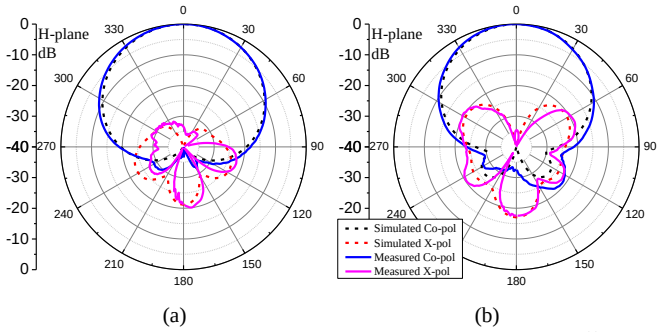

Fig. 12. Simulated and measured H-plane radiation patterns when differential port d1 is excited. (a) 3.2 GHz. (b) 3.7 GHz.

IV. Results and Discussion

A. Antenna Element

The proposed differentially driven dual-polarized antenna element was fabricated and measured. All the antenna and array were measured by the Rohde & Schwarz ZVL network analyzer and the Asysol far field antenna measurement system at the University of Kent. The fabricated antenna prototype is shown in Fig. 10, and the measured S-parameters are shown in Fig. 11. It can be seen that the measured S-parameters agree well with the simulated results. The measured bandwidth for S_{dd11} and S_{dd22} below -10 dB is 3.17-3.77 GHz, and the isolation between the two differential ports is higher than 38.5 dB. Discrepancies between the simulated and measured results are mainly due to the fabrication and assembly errors.

Fig. 12 shows the measured and simulated normalized radiation patterns for the proposed antenna in the H-plane when differential port d1 is driven. Owing to the symmetry of the antenna, only H-plane radiation patterns are given in the figure. The measured half-power beamwidth in the H-plane is about 65º. The measured cross-polarization level is lower than -33 dB in the broadside direction. Good agreement can be observed between the simulated and measured radiation patterns. The measured peak realized gain is

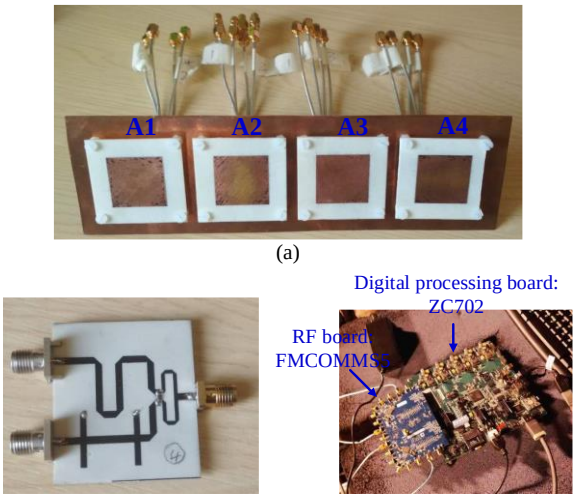

Fig. 13. Protographs of (a) the fabricated 1 × 4 antenna array, (b) the fabricated out-of-phase power divider, and (c) the hardware platform for beam scanning performance.

about 8.2 dBi within the bandwidth, which is 1.2 dB lower than the simulated peak realized gain.

B. Antenna Array

Fig. 13 shows the photographs of the fabricated 1×4 antenna array, an out-of-phase power divider, and a generic hardware platform. The out-of-phase power divider is used to feed differentially driven antenna for radiation patterns measurement. The generic hardware platform, which is composed of a digital processing board ZC702 and a RF board FMCOMMS5, is used to generate the desired scanning beams. The measured S-parameters of the antenna element in the array are shown in Fig. 14. The measured overlapped 15 dB return loss bandwidth is from 3.3 GHz to 3.66 GHz. The measured isolation is better than 35 dB. The isolation in the array is a little worse than the antenna element, which is caused by the fabrication errors and the mutual couplings from the other antenna elements.

Fig. 15 shows the measured and simulated radiation patterns of the antenna array when each antenna element is excited with equal magnitude and co-phase signal at 3.3 GHz and 3.6 GHz. Because of the symmetry of the two polarizations, only radiation patterns excited by the differential port d1 are given in the figure. In the H-plane, the beamwidth is 66-70º within the bandwidth. In the V-plane, the maximum radiation direction is observed in the +z direction, and the beamwidth is 20-22º within the bandwidth. Due to the mutual coupling between the antenna elements, the measured the cross-polarization level is -20.8 dB lower than the co-polarization in the broadside direction. The measured back lobe level is better than the simulated result, which is probably caused by the blockage of the feeding coaxial cables. The measured realized peak gain of the antenna array is around 13.8 dBi.

Because the antenna array is measured with the array beamwidth of 20-22º, three beams with the scan angles of -20º, 0º, and +20º are investigated. As shown in Fig. 16, with the beam scanning performance, the measured overall half-power beamwidth of the three beams can cover 64º and 61º at 3.3 GHz and 3.6 GHz. The measured cross-polarization levels are lower than the broadside beam when the array beam scans at ±20º, which are lower than -24 dB. The measured realized gain at the scan angles of ±20º is about 0.4 dB lower than the broadside beam. Therefore, the beam scanning

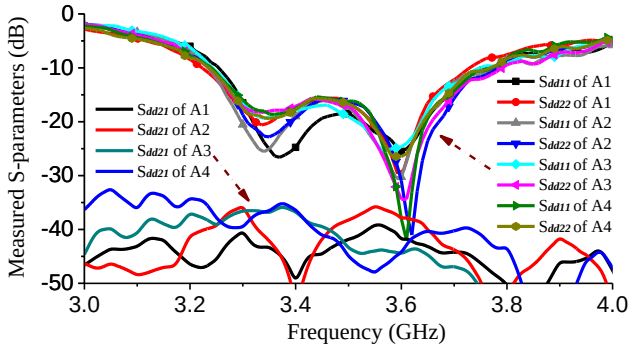

Fig. 14. Measured S-parameters of the four antenna elements in the fabricated 1×4 antenna array.

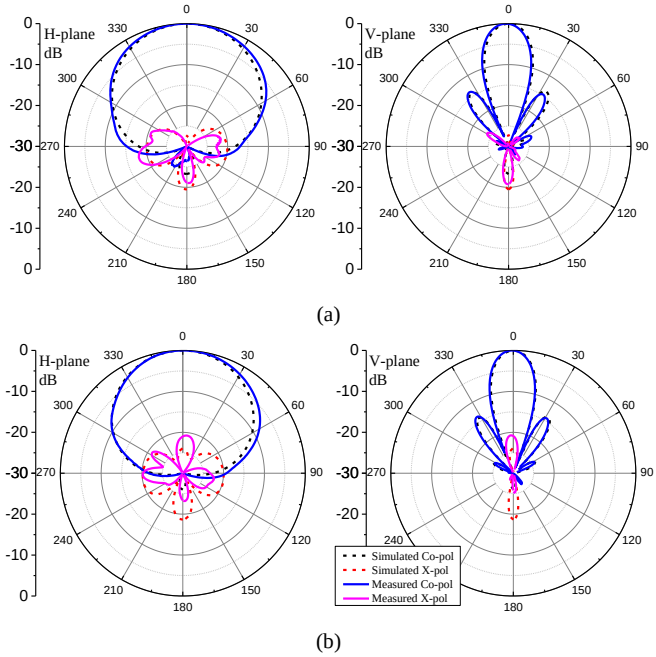

Fig. 15. Simulated and measured radiation patterns when the differential port d1 is excited for the fabricated antenna array. (a) 3.3 GHz. (b) 3.6 GHz.

performance of the proposed antenna array can provide a good coverage for base stations.

C. Comparison

Table I compares the performances of the proposed wideband antenna with the recently published dual-polarized patch antennas. In the table, λ_0 is the free space wavelength at the center operation frequency. Designs in [4]-[5] are the single-ended dual-polarized antennas, and they have the moderate port isolation and cross-polarization level. Antennas in [16] and [21]-[23] are driven by the differential method, and high port isolation is achieved. However, high antenna port isolation does not promise the low cross-polarization level. Although antenna in [16] has the widest impedance bandwidth, its profile is the largest. By using 180º ring hybrid coupler, the dual-polarized antenna in [23] obtains highest port isolation and lowest cross-polarization level. However, additional insertion loss is introduced with a very narrow bandwidth. By using the open loop resonators, our proposed antenna achieves a wide impedance bandwidth, and keeps low profile configuration. Moreover, high isolation (>38.5 dB) and low cross-polarization level (<-33 dB) are also obtained simultaneously. In terms of the fabrication cost, multi-layer PCB technology is normally used to

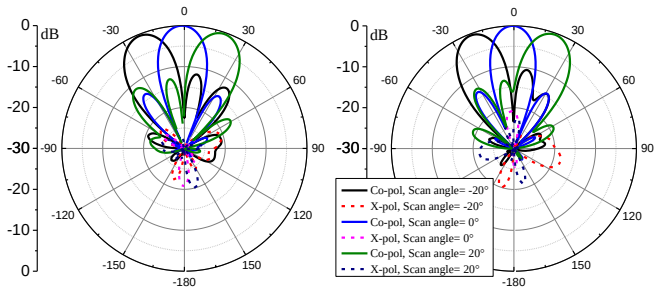

(a) (b)

Fig. 16. Measured radiation patterns with the scan angles of -20º, 0º, and +20º. (a) 3.3 GHz. (b) 3.6 GHz.

TABLE I
COMPARISON OF THE REFERENCE ANTENNAS

Ref.	FBW	Height	Isolation (dB)	X-pol (dB)	Driven Mode	No. of Substrates	No. of Layers
[4]	3.6%	$0.1\lambda_0$	25	-19.5	Single	2	4
[5]	26.7%	$0.2\lambda_0$	25	-20	Single	2	3
[16]	49.4%	$0.27\lambda_0$	37	-21	Dif.	2	3
[21]	19%	$0.08\lambda_0$	35	-16	Dif.	3	4
[22]	18.8%	$0.08\lambda_0$	35	-20	Dif.	2	4
[23]	2%	$0.025\lambda_0$	62	-50	Dif.	1	2
This work	17.2%	$0.067\lambda_0$	38.5	-33	Dif.	1	1

realize wideband patch antennas, which increase the fabrication complexity and cost. Compared to the other reference antennas, the presented design only uses one substrate with one layer to print the radiator. Therefore, our proposed antenna is especially competitive with the simple structure and low fabrication cost.

V. CONCLUSION

This communication presents a novel low-cost differentially driven dual-polarized antenna. Novel intersected open loop resonators are used to excite the top radiating patch with electric coupling. Owing to the even mode and odd mode current distributions on the resonators, high port isolation and low cross-polarization level are achieved with wide impedance bandwidth and compact size. For the presented antenna, impedance bandwidth of 17.2% is measured with the thickness of $0.067\lambda_0$. Furthermore, high isolation (>38.5 dB) and low cross-polarization (<-33 dB) are also achieved. One linear antenna array is designed for 5G base station applications with very low reflection coefficient (<-15 dB). Beam scanning performance is investigated to provide the required base station coverage. Both the simulated and the measured results prove that the proposed antenna can be a good candidate for wireless communication systems with a simple configuration and low fabrication cost.

REFERENCES

[1] K. L. Wong, *Compact and Broadband Microstrip Antennas.* Hoboken, NJ, USA: Wiley, 2002

[2] S.-C. Gao, L.-W. Li, M.-S. Leong, and T.-S. Yeo, "Dual-polarized slot coupled planar antenna with side bandwidth," *IEEE Trans. Antennas Propag.*, vol. 51, no. 3, pp. 441–448, Mar. 2003.

[3] S. Gao, L. W. Li, M. S. Leong, and T. S. Yeo, "A broad-band dual-polarized microstrip patch antenna with aperture coupling," *IEEE Trans. Antennas Propag.*, vol. 51, no. 4, pp. 898–900, Apr. 2003.

[4] H. Li, L. Kang, F. Wei, Y. M. Cai, and Y. Z. Yin, "A low-profile dual-polarized microstrip antenna array for dual-mode OAM applications," *IEEE Antennas Wirel. Propag. Lett.*, vol. 16, pp. 3022–3025, 2017.

[5] Y. Wang and Z. Du, "Dual-polarized slot-coupled microstrip antenna array," *IEEE Trans. Antennas Propag.*, vol. 63, no. 9, pp. 4239–4244, 2015.

[6] H. W. Lai and K. M. Luk, "Dual polarized patch antenna fed by meandering probes," *IEEE Trans. Antennas Propag.*, vol. 55, no. 9, pp. 2625–2627, 2007.

[7] J.-J. Xie, X.-S. Ren, Y.-Z. Yin, and J. Ren, "Dual-polarised patch antenna with wide bandwidth using electromagnetic feeds," *Electron. Lett.*, vol. 48, no. 22, p. 1385, 2012.

[8] J. Y. Deng, L. X. Guo, Y. Z. Yin, J. Qiu, and Z. Sen Wu, "Broadband patch antennas fed by novel tuned loop," *IEEE Trans. Antennas Propag.*, vol. 61, no. 4, pp. 2290–2293, 2013.

[9] L. Wen *et al.*, "Compact Dual-Polarized Shared-Dipole Antennas for Base Station Applications," *IEEE Trans. Antennas Propag.*, vol. 66, no. 12, pp. 6826-6834, Dec. 2018.

[10] H. Huang, Y. Liu, and S. Gong, "A novel dual-broadband and dual-polarized antenna for 2G / 3G / LTE base stations," vol. 64, no. 9, pp. 4113–4118, 2016.

[11] H. Sun, C. Ding, B. Jones and Y. J. Guo, "A Wideband Base Station Antenna Element With Stable Radiation Pattern and Reduced Beam Squint," *IEEE Access*, vol. 5, pp. 23022-23031, 2017.

[12] B. Li, Y. Z. Yin, W. Hu, Y. Ding, and Y. Zhao, "Wideband dual-polarized patch antenna with low cross polarization and high isolation," *IEEE Antennas Wirel. Propag. Lett.*, vol. 11, pp. 427–430, 2012.

[13] B. Q. Wu and K. M. Luk, "A broadband dual-polarized magneto-electric dipole antenna with simple feeds," *IEEE Antennas Wirel. Propag. Lett.*, vol. 8, pp. 60–63, 2009.

[14] Y. Cui, R. L. Li, and P. Wang, "A novel broadband planar antenna for 2G/3G/LTE base stations," *IEEE Trans. Antennas Propag.*, vol. 61, no. 5, pp. 2767–2774, 2013.

[15] L. Wen *et al.*, "A Wideband Dual-Polarized Antenna Using Shorted Dipoles," *IEEE Access*, vol. 6, pp. 39725-39733, 2018.

[16] Z. Tang, J. Liu, Y. M. Cai, J. Wang, and Y. Yin, "A Wideband Differentially Fed Dual-Polarized Stacked Patch Antenna with Tuned Slot Excitations," *IEEE Trans. Antennas Propag.*, vol. 66, no. 4, pp. 2055–2060, 2018.

[17] C. H. K. Chin, Q. Xue, and H. Wong, "Broadband patch antenna with a folded plate pair as a differential feeding scheme," *IEEE Trans. Antennas Propag.*, vol. 55, no. 9, pp. 2461–2467, 2007.

[18] A. Wu, B. Guan, and Z. Zhang, "A novel WiMAX patch antenna," *IEEE Antennas Wirel. Propag. Lett.*, vol. 5, pp. 1–4, 2006.

[19] T. S. P. See, W. Liu, X. Qing, and Z. N. Chen, "A wideband differential directional antenna for head implants," *IEEE Trans. Antennas Propag.*, vol. 63, no. 7, pp. 3244–3248, 2015.

[20] H. Jin, K. S. Chin, W. Che, C. C. Chang, H. J. Li, and Q. Xue, "Differential-fed patch antenna arrays with low cross polarization and wide bandwidths," *IEEE Antennas Wirel. Propag. Lett.*, vol. 13, pp. 1069–1072, 2014.

[21] X. Yang, L. Ge, J. Wang, and C. Sim, "A Differentially-Driven Dual-Polarized High-Gain Stacked Patch Antenna," *IEEE Antennas Wirel. Propag. Lett.* vol. 17, no 7. pp. 1181-1185, 2018.

[22] C. Deng, S. Member, Y. Li, Z. Zhang, and S. Member, "A Wideband High-Isolated Dual-Polarized Patch," *IEEE Antennas Wirel. Propag. Lett.*, vol. 13, pp. 1617–1619, 2015.

[23] H. Nawaz and I. Tekin, "Dual-Polarized, Differential Fed Microstrip Patch Antennas With Very High Interport Isolation for Full-Duplex Communication," *IEEE Trans. Antennas Propag.*, vol. 65, no. 12, pp. 7355–7360, 2017.

[24] W. R. Eisenstadt, B. Stengel, and B. M. Thompson, *Microwave Differential Circuit Design Using Mixed-Mode S-Parameters*. Boston, MA, USA: Artech House, 2006

[25] C. Mao, S. Gao, Y. Wang, F. Qin and Q. Chu, "Multimode Resonator-Fed Dual-Polarized Antenna Array With Enhanced Bandwidth and Selectivity," *IEEE Trans. Antennas Propag.*, vol. 63, no. 12, pp. 5492-5499, Dec. 2015.

[26] J. S. Hong and M. J. Lancaster, *Microstrip Filters for RF/Microwave Applications*. New York, NY, USA: Wiley, 2001.

[27] C. A. Balanis, *Antenna Theory: Analysis and Design*, 3rd ed. New York, NY, USA: Wiley, 2005